Biomimic Light Trapping Silicon Nanowire Arrays for Laser Desorption/Ionization of Peptides

ARTICLE *in* THE JOURNAL OF PHYSICAL CHEMISTRY C · JUNE 2012

Impact Factor: 4.77 · DOI: 10.1021/jp3034402

THE JOURNAL OF PHYSICAL CHEMISTRY C

Article

pubs.acs.org/JPCC

Biomimic Light Trapping Silicon Nanowire Arrays for Laser Desorption/Ionization of Peptides

Chaoming Wang,[†] Jennifer M. Reed,[‡] Liyuan Ma,*[,†] Yong Qiao,[†] Yang Luo,[†] Shengli Zou,[‡] James J. Hickman,[†] and Ming Su[†]

[†]NanoScience Technology Center, [‡]Department of Chemistry, University of Central Florida, Orlando, Florida 32826, United States

ABSTRACT: This article describes a low cost method of generating silicon nanowire arrays that have similar structure and light trapping ability as moth-eye for matrix-free laser desorption/ionization mass spectrometry analysis of small molecules without matrix peak interference. The nanowire array is produced by combining low cost nanosphere lithography and metal nanoparticle-assisted chemical etching of silicon. Owing to their excellent light trapping ability over broad spectral range, silicon nanowire arrays can absorb incoming laser light efficiently, and convert laser energy to heat, which allows efficient desorption/ionization of intact peptide/proteins without matrix. Compared to existing matrix-free substrate such as porous silicon substrates, the biomimic silicon nanowire arrays are better in terms of lower laser energy, structural tunability, and low spatial resistance.

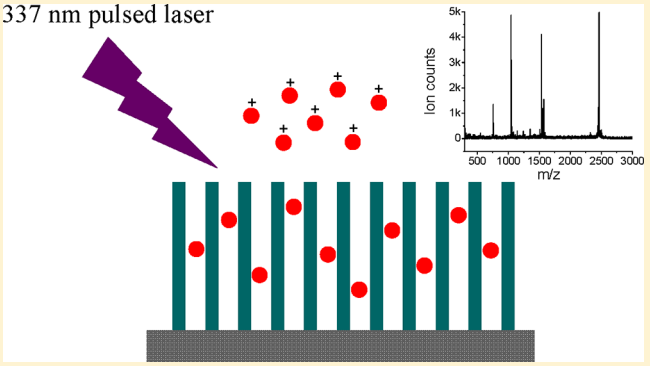

1. INTRODUCTION

Mass spectrometry is powerful in analyzing biomolecules such as peptides, proteins, and oligonucleotides by forming molecular ions that are separated according to their charge to mass ratio.[1,2] Among existing ionization methods, laser can be controlled easily and allows ionization from a small spot for high throughput analysis, but , direct ionization requires high intensity laser that can lead to ion fragmentation. Laser absorbing matrixes (α-cyano-4-hydroxycinnamic acid, sinapinic acid, and 2,5-dihydroxybenzoic acid) can be mixed with analytes to assist desorption and ionization of proteins or peptides without causing fragmentation as in matrix-assisted laser desorption/ionization mass spectrometry (MALDI-MS).[3−5] MALDI-MS allows direct analysis of thermal labile proteins, but small molecules including short peptides (MW < 600 Da) cannot be analyzed directly with MALDI-MS due to strong matrix signals at low molecular weight region, which limits the ability in studying small molecules that play important roles in cellular functions, finding biomarkers, and detecting diseases, and their interactions with proteins.[6−10]

Laser desorption/ionization of protein combines three sequential steps: laser absorption, light-to-heat conversion, and ion desorption/ionization.[11] In order to eliminate matrix effect, a variety of matrix-free techniques have been used to achieve low optical reflection, efficient light-to-heat conversion, excellent electrical conductivity, large surface area to retain enough analytes, and open access so that desorbed ions can leave with minimal restriction.[12] Nanostructures that have unique optical, electrical, and thermal properties and large surface areas have been used to ionize small molecules including peptides for matrix free laser desorption/ionization. Porous silicon substrates derived from electrochemical etching gain popularity due to large surface area, and good electrical conductivity.[13−16] However, the intertwined structures in porous silicon retard desorption of ionized analytes, and high laser energy is required to produce a large number of ions. High density array of vertical silicon nanowires or carbon nanotubes made by chemical vapor deposition have also been used for matrix free ionization of proteins,[17−19] but carbon nanotubes are hydrophobic and have large water contact angle that prevents spreading of aqueous solution, leading to the formation of an aggregated cluster of analytes; in the case of silicon nanowires (diameter of ∼50 nm), the substrate is normally gray, and the light trapping ability is not significant, which means a certain portion of the laser energy is reflected. In addition, it is also difficult to make silicon nanostructures with reproducible performance at low cost using existing methods, which leads to spot-to-spot or batch-to-batch variation in porous structure (size or depth) and nanowire structure (diameter, length, or density).

Light hit on a substrate can be reflected and absorbed. It has been shown that the larger the difference in refractive indices between two media, the greater the proportion of light that will be reflected.[20] If the surface is textured with an array of subwavelength grooves or ridges, the difference between the indices of refraction of texture and air is significantly reduced, and such a region can act as a single layer antireflective coating. The antireflective effect can be largely enhanced by multi-

Received: April 10, 2012
Revised: June 22, 2012
Published: June 25, 2012

dx.doi.org/10.1021/jp3034402 | J. Phys. Chem. C 2012, 116, 15415−15420

layered antireflection coating with each successive layer designed to provide destructive interference at different wavelengths.[21,22] Thin film of multilayers that have different refractive indices has been produced to reduce light reflectance. In nature, night-flying moths use submicrometer surface textures in their eyes to reduce reflected light to avoid being visible to their predators.[23] Electron microscopy observation of moth-eye has shown an array of vertically aligned nanocones that change effective refractive indices between those of air and eye gradually, reducing reflection and greatly enhancing absorption of incident light. Ever since its discovery, light trapping moth-eye structure has inspired numerous researches in producing antireflective structures, but in order to obtain antireflective properties over ultraviolet to visible wavelength from 300 to 700 nm, high-resolution fabrication techniques such as electron beam lithography and interference lithography will have to be used. In addition, it is expensive and time-consuming to make such submicrometer structures over a sufficiently large array on silicon substrate using high-resolution lithography techniques.

This article reports a low cost, reproducible method of making vertically aligned silicon nanowire arrays that have extremely high light trapping ability for matrix-free laser desorption/ionization of peptides with high efficiency. The silicon nanowire arrays are generated by combining low cost nanosphere lithography and metal nanoparticle-assisted chemical etching of silicon. Figure 1 shows procedures of making

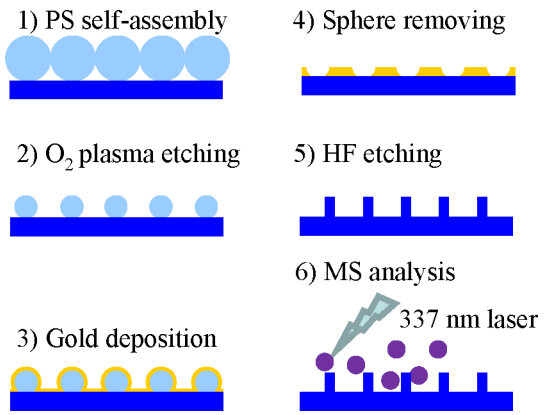

Figure 1. Ordered silicon nanowire arrays fabricated by using nanosphere lithography for laser desorption/ionization mass spectrometry.

silicon nanowire arrays: (1) polystyrene nanospheres are self-assembled over a large area of silicon substrate to form a closely packed monolayer; (2) oxygen plasma etching is used to reduce nanosphere size; (3) a thin film of gold is evaporated on silicon substrate using size-reduced nanospheres as shadow mask; (4) after removing polystyrene nanospheres, an ordered array of nanoholes is produced in gold film; (5) subsequently, silicon substrate underlying gold film is chemically etched using gold film as catalyst, which generates an ordered array of vertically aligned silicon nanowires. The structures of silicon nanowires including diameter, spacing, and length could be tuned by adjusting experimental conditions such as size of nanospheres and etching condition. The nanostructured silicon substrate has excellent light trapping ability over a broad wavelength range from visible to ultraviolet region, superior electrical conductivity of doped silicon, large water contact angle (hydrophobic to avoid analyte spreading), large surface area (to allow analyte retention), and open space (to allow charged ions to desorb), thus permitting efficient laser desorption/ionization of analytes.

2. EXPERIMENTAL SECTION

All chemicals were reagent grade and used without further purification. Surfactant-free and carboxyl-modified polystyrene suspension (400 nm diameter) was obtained from Invitrogen (Carlsbad, CA), which contains 4% solid. Silicon substrates (p-type boron-doped, resistivity of 8−25 Ω cm^{-2}) were obtained from University Wafer (South Boston, MA). Hydrogen peroxide (H_2O_2), sulfuric acid (H_2SO_4), ammonium hydroxide (NH_4OH), hydrogen fluoride (HF), and acetonitrile (ACN) were obtained from VWR (West Chester, PA). Standard peptides including bradykinin fragment 1−7 (MW757), angiotensin-II (MW1046), synthetic peptide P14R (MW1534), and adrenocorticotropic hormone (ACTH) fragment (MW2464) were from Sigma-Aldrich (St. Louis, MO). α-Cyano-4-hydroxycinnamic acid (CHCA), trifluoroacetic acid (TFA), and methanol were purchased from Sigma-Aldrich (St. Louis, MO). Stock solutions were prepared by reconstituting lyophilized powder in distilled water. Samples were diluted in methanol/0.1% TFA (30:70, v/v). One microliter aliquots were pipetted directly on silicon nanowire substrate, and dried at room temperature to generate spots of 2 mm in diameter. High-purity gold pellets (99.99%) were purchased from Goodfellow (Oakdale, PA) and used as the source in thermal evaporation. Ultrapure water with resistivity of 18.2 MΩ·cm was obtained from a Millipore system (Marlborough, MA) and used to clean silicon surfaces and make solutions.

Silicon substrate was treated in piranha solution that contained 3:1 (v/v) concentrated H_2SO_4 and 30% H_2O_2 at 80 °C for 1 h, and rinsed with deionized water to remove contamination. The substrate was sonicated in 5:1:1 (v/v) $H_2O/NH_4OH/H_2O_2$ for 1 h and washed with a large amount of deionized water. After treatment, the substrates become hydrophilic due to production of hydroxyl groups. A droplet (2 μL) of solution of nanospheres at original concentration was dropped on a silicon substrate, and the substrate was rotated for a few minutes until nanospheres were uniformly dispersed inside water film. The substrate was stored under a covered Petri dish until water evaporated completely. After reducing the size of polystyrene nanospheres with oxygen plasma etching, the nanosphere monolayer was used as a shadow mask to form gold nanoholes, which were then used as catalyst to etch silicon to form silicon nanowires. A thermal evaporator (Denton) was used to deposit gold thin film onto patterned substrate in vacuum with pressure lower than 5.0×10^{-6} Torr. Following gold deposition, polystyrene nanospheres were removed by dissolution in chloroform ($CHCl_3$) to create an ordered array of nanoholes, whose diameters were determined by size-reduced polystyrene nanospheres. At last, silicon under gold thin film was catalytically etched in a mixture of deionized water, 10 wt % HF, and 1.5 wt % H_2O_2 and rinsed by using ethanol and deionized water, respectively. An optical microscope (Olympus, BX51M) was used to image bare silicon substrates, nanosphere covered silicon substrate, and silicon nanowires. A scanning electron microscope (Zeiss Ultra 55 SEM) operated at voltage of 10 kV was used to collect high-resolution images of silicon nanowire arrays. The surface contact angle of substrate was measured by using a Ramé-Hart model 250 standard contact angle goniometer (Succasunna,

dx.doi.org/10.1021/jp3034402 | J. Phys. Chem. C 2012, 116, 15415−15420

NJ). A mini-spectrometer (USB 4000, Ocean Optics) coupled with optical fiber is used to measure total reflectance in ultraviolet to visible range.

A peptide mixture of bradykinin fragment 1−7, angiotensin-II, P14R, and ACTH fragment of 10 pmol/μL concentration each was made in 0.1% TFA in purified water. A series of dilutions was made to achieve the final solution with 1 pmol/μL peptide concentrations. Four microliters of this mixture was mixed with 1 μL of matrix solution to make the total volume 5 μL. The matrix solution was made as follows: a saturated solution of α-cyano-4-hydroxy-*trans*-cinnamic acid in acetonitrile was diluted 10 times with 1:1 (v/v) mixture of ACN and 0.1% TFA water. Five microliters of sample/matrix mixture was applied to anchor chip and allowed to dry. In a control experiment, the same amount of peptides (2 μL) was pipetted to conventional MALDI target. Laser desorption/ionization mass spectrometric analysis was carried out with an Applied Biosystems (Framingham, MA) Voyager DE Pro time-of-flight mass spectrometer that was operated with pulsed nitrogen laser at 337 nm at a repetition rate of 20 Hz. The nanostructured substrate (area of 1 cm^2) was attached onto a modified target plate using double-side conductive tape. Positive ion mode mass spectra were obtained in linear mode with acceleration potential of 20 kV and a grid of voltage at 74%. Each spectrum was obtained from 100 averaged laser pulses. Signal-to-noise ratios were derived with Voyager Data Explorer version 4.0 (Applied Biosystems, Framingham, MA, USA).

3. RESULTS AND DISCUSSION

3.1. Self-Assembled Polystyrene Nanospheres Monolayer. Carboxylic modified polystyrene nanospheres assembled on the silicon substrate to form a closely packed hexagonal pattern. The process was driven by lateral capillary force of liquid−solid contact line on nanospheres. The film thickness was correlated with its optical characters, allowing a facile and quick quality control. Figure 2 showed optical micrographs and according scanning electron microscope (SEM) images of nanosphere films. The low magnification optical image showed coexistence of nanosphere films of different thicknesses with different contrast (2A). In the high magnification images (Figure 2B−D), green, gray, and blue regions were found to be from single layer, multilayer, and under-packed single layer, respectively, where different colors were induced by light diffraction over nanospheres.

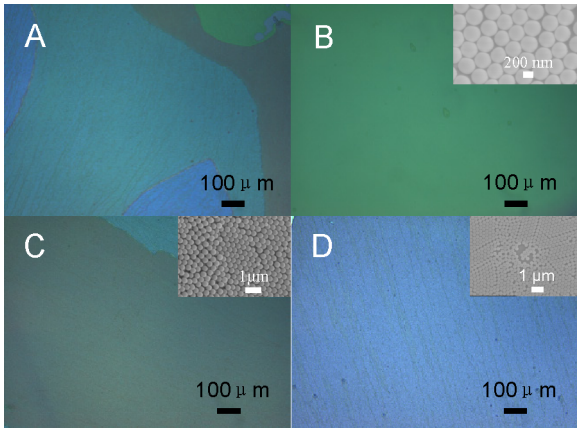

Figure 2. Typical optical micrograph image of polystyrene nanospheres film (A); the green, gray, and blue regions are from single layer (B), multilayer (C), and under-packed single layer spheres (D), respectively.

3.2. Vertically Aligned Silicon Nanowire Arrays. The nanosphere monolayer coated silicon substrates were treated with oxygen plasma for various times ranging from 5 to 15 min to reduce the size of polystyrene nanospheres and generate a shadow mask for metal deposition. Figure 3 was SEM images of

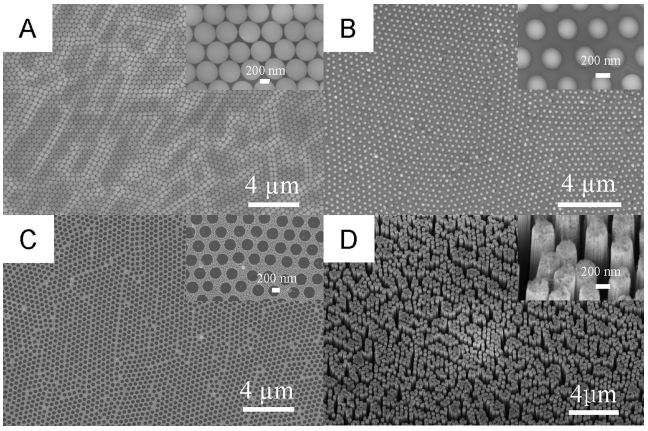

Figure 3. SEM images of closed-packed nanospheres on silicon surface before (A) and after (B) oxygen plasma etching; an ordered array of nanoholes after removing nanospheres (C); vertical silicon nanowire arrays made after catalytically etching silicon with gold (D).

the nanosphere monolayer before (A) and after plasma treatment (B), where the diameters of nanospheres were reduced from 400 to 200 nm after 10 min of treatment. Subsequently, a 10 nm gold film was deposited onto this patterned substrate. Then, polystyrene nanospheres were removed by dissolution in chloroform ($CHCl_3$) to form an ordered array of gold nanoholes with diameters determined by size-reduced polystyrene nanospheres (C). Silicon under gold thin film was catalytically etched in a mixture of deionized water, 10 wt % HF, and 1.5 wt % H_2O_2 for varied times, and rinsed with ethanol and deionized water for 20 s. The etching step generated vertically aligned silicon nanowires as in the SEM image (D), where the interwire space and height of nanowires were 400 and 2000 nm, respectively. The surface area of silicon nanowires over a 1 cm^2 area was determined to be 10 cm^2. The high resolution image showed that each nanowire had a rough side wall, which could enhance light trapping. The large surface-to-volume ratio was crucial for laser absorption, and open space between nanowires allows easy desorption of analytes without restriction. The nanowire array had water contact angle of 107°, which confined aqueous solution of analyte in a small region, increasing concentration of analytes in a dry spot. The silicon substrate with nanowires had similar resistivity (10 ± 0.5 ohm·cm) as original silicon substrate (12 ± 0.5 ohm·cm) and thus can dissipate electrical charges generated in laser desorption.

3.3. Light Trapping on Vertically Aligned Silicon Nanowire Arrays. The light trapping ability of silicon nanowires was examined in total reflectance mode in the ultraviolet to visible range. A clean and flat silicon substrate was used as a control. An incident light (beam size of 2 mm^2) was directed on the flat silicon and nanostructured silicon surface. Figure 4A,B were optical micrographs of a flat substrate and nanowire arrays, respectively. The black surface confirmed that most incoming light was trapped by silicon nanowires, and

dx.doi.org/10.1021/jp3034402 | J. Phys. Chem. C 2012, 116, 15415−15420

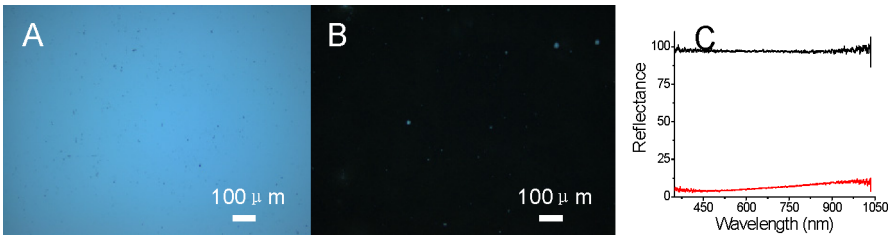

Figure 4. Optical images of flat silicon (A) and silicon nanowire arrays (B); light reflectance as a function of wavelength of the flat silicon substrate (black) and silicon nanowire arrays (red) (C).

almost no light was reflected to the optic microscope. The light antireflection/trapping ability of silicon nanowires was quantified by measuring reflectance in normal incident angle. Figure 4C was the reflectance of flat (black) and nanostructured (red) silicon substrates as a function of wavelength from 330 to 800 nm, where the reflection of flat silicon substrate was set at 100%. Silicon nanowire arrays absorbed most of the incoming light with 99.99% absorbance even into ultraviolet range.

The optical spectra of silicon nanowire arrays were simulated by using the discrete dipole approximation (DDA) method,[24] and light trapping was simulated using the ray-tracing method in which the scattering of light from ultraviolet to visible range in nanowires was derived. In the simulations, nanowires were modeled with a height of 2 μm and diameters of 200 and 50 nm, respectively. The nanowires were arranged in a hexagonal array with a center-to-center spacing of 400 nm. The incident light propagated along symmetric axis of nanowire. Figure 5A showed the absorption (red) and scattering spectra (black) of 200 nm diameter silicon nanowires, where 90% of light in the 380−400 nm range was trapped, and reflection was less than 5% at most wavelengths. At the wavelength of 337 nm, the reflection was close to zero. In addition, the electric field $|E|^2$ distribution at 337 nm was derived (Figure 5B). The intensity

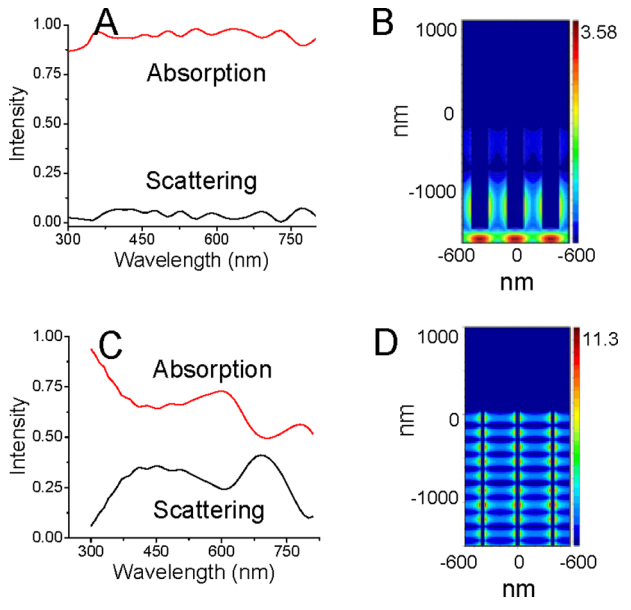

Figure 5. Simulated absorption (red) and scattering (black) spectra of silicon nanowire arrays with nanowire diameter of 200 nm (A) and 50 nm (C); simulated electric field distributions on nanowire arrays at 337 nm laser excitation with nanowire diameter of 200 nm (B) and 50 nm (D), respectively.

of light decayed quickly once entering the silicon nanowire array. The complete trapping of incoming laser photons had generated a large amount of heat, which was transferred to analytes to cause ionization and desorption of ionized analytes into gas phase. The nanowire diameters played a role in light trapping as well. Similar simulation had been done with nanowire diameter of 50 nm while keeping other parameters the same. The result indicated that the laser absorption dropped, while scattering increased for 50 nm nanowires (Figure 5C). The electric field distribution also showed that light intensity did not decay as quickly as that of the 200 nm nanowire (Figure 5D). In summary, these data suggest that the vertical array of 200 nm diameter nanowires had higher light trapping ability than 50 nm diameter nanowires.

3.4. Matrix-Free Laser Desorption/Ionization. Figure 6A showed LDI-MS spectra of the peptide mixture deposited onto silicon nanowire arrays. The ultralow background in low mass range (<400 Da) confirmed complete elimination of matrix peaks, and the strong peptide peaks confirmed matrix-free desorption/ionization from silicon nanowire arrays. In control experiments with unmodified silicon substrate, no peptide signals were observed at the same laser irradiation condition (spectrum not shown), excluding the possibility of direct laser degradation or fragmentation of peptides. The peptide mixture had also been tested on commercial desorption/ionization on silicon (DIOS) substrate obtained from Waters (Milford, MA) (Figure 6B). A peptide with high molecular weight (2,500 kDa) had very low peak intensity on the DIOS substrate, which was likely due to the larger ions requiring much more energy to desorb. The silicon nanowire arrays can trap laser light efficiently, and allow efficient desorption of large ions. The peptide mixture had also been tested with normal MALDI analysis using the α-cyano-4-hydroxycinnamic acid as matrix (Figure 6C). The silicon nanowire arrays had same strong signals as that of MALDI analysis with matrix but without the overwhelming matrix peak interference below 500 Da.

3.5. Low Energy Laser Desorption/Ionization. Low laser energy was preferred in desorption and ionization to preserve intact protein or peptide structures. Since each spectrum in Figure 6 was collected at 100 laser pulses, the efficiency of ionization/desorption could then be compared to each other. Each laser pulse can generate 15−50 ions on silicon nanowire array, 2−20 ions on DIOS substrate and 5−40 ions with matrix. The energy of each pulse was 170 μJ, which results in a peak power of 45 kW and an average power of 3 mW. Figure 6D was the relative ratios of ions generated from silicon nanowire array and DIOS substrate, where the discrepancy was induced by a structural difference between them. The ordered silicon nanowire surface had larger light trapping ability than that of the random structured DIOS substrate. In addition, the

dx.doi.org/10.1021/jp3034402 | J. Phys. Chem. C 2012, 116, 15415−15420

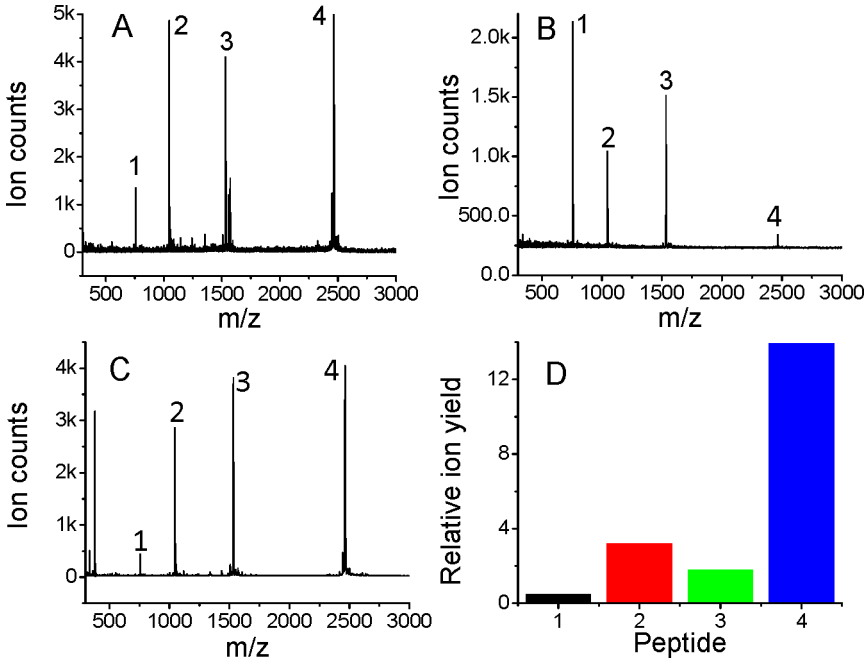

Figure 6. LDI-MS of peptide mixture using silicon nanowire arrays (A) and DIOS substrate (B); MALDI-MS of the same peptide mixture using α-cyano-4-hydroxycinnamic acid as the matrix (C); relative yields of four peptide ions on silicon nanowire array and DIOS substrate (D), where data are derived from panels A and B.

silicon nanowire arrays had an open space, so that ionized molecules can be desorbed quickly into the gaseous phase. Larger molecules experienced more spatial resistance than smaller ones on porous silicon. Although the yields of molecular ions on a silicon nanowire array were comparable to those with a matrix, the presence of matrix peaks was not ideal for many studies especially those related to small molecules.

4. CONCLUSIONS

This study had developed a low cost method of making silicon nanowire arrays and using the array for low energy matrix-free laser desorption/ionization mass spectrometry. The low laser energy was the result of several structural characters: (1) enhanced laser absorption in ultraviolet range; (2) abundant proteins absorbed on hydrophobic silicon nanowires that had large surface area; (3) open interwire space that allowed easier desorption of ionized proteins; and (4) electrical conductivity of nanostructured silicon substrate. The method of making a nanostructured substrate by combining nanosphere lithography and gold catalyzed chemical etching was cheap and could be scaled up to the centimeter scale. The nanostructured silicon substrate was robust, making it an ideal substrate for next generation matrix free laser desorption/ionization.

AUTHOR INFORMATION

Corresponding Author

*E-mail: liyuanma@mail.ucf.edu.

Notes

The authors declare no competing financial interest.

ACKNOWLEDGMENTS

This work was supported by a New Investigator Research Grant (to L. Ma) from Bankhead-Coley Cancer Research Program of Florida Department of Health. All characterization works were done in NanoScience Technology Center (NSTC) and Materials Characterization Facility (MCF) of University of Central Florida (UCF). S. Zou thanks NSF, ONR, and ACS/PRF for the support of research.

REFERENCES

(1) Cohen, L. H.; Gusev, A. I. Small molecule analysis by MALDI mass spectrometry. *Anal. Bioanal. Chem.* **2002**, *373*, 571.

(2) Anker, J. N.; Hall, W. P.; Lambert, M. P.; Velasco, P. T.; Mrksich, M.; Klein, W. L.; Van Duyne, R. P. Detection and identification of bioanalytes with high resolution LSPR spectroscopy and MALDI mass spectrometry. *J. Phys. Chem. C* **2009**, *113*, 5891.

(3) Tholey, A.; Heinzle, E. Ionic (liquid) matrices for matrix-assisted laser desorption/ionization mass spectrometry-applications and perspectives. *Anal. Bioanal. Chem.* **2006**, *386*, 24.

(4) Karas, M.; Hillenkamp, F. Laser desorption ionization of proteins with molecular masses exceeding 10,000 Da. *Anal. Chem.* **1988**, *60*, 2299.

(5) Spencer, M. T.; Furutani, H.; Oldenburg, S. J.; Darlington, T. K.; Prather, K. A. Gold nanoparticles as a matrix for visible-wavelength single-particle matrix-assisted laser desorption/ionization mass spectrometry of small biomolecules. *J. Phys. Chem. C* **2008**, *112*, 4083.

(6) Hashir, M. A.; Stecher, G.; Bakry, R.; Kasemsook, S.; Blassnig, B.; Feuersein, I.; Abel, G.; Popp, M.; Bobleter, O.; Bonn, G. K. Identification of carbohydrates by matrix-free material-enhanced laser desorption/ionisation mass spectrometry. *Rapid Commun. Mass Spectrom.* **2007**, *21*, 2759.

(7) Rivkin, A.; Chou, T. C.; Danishefsky, S. J. On the remarkable antitumor properties of fludelone: how we got there. *Angew. Chem., Int. Ed.* **2005**, *44*, 2838.

(8) Rochfort, S. Metabolomics reviewed: a new "Omics" platform technology for systems biology and implications for natural products research. *J. Nat. Prod.* **2005**, *68*, 1813.

(9) Smith, C. A.; Maille, G. O.; Want, E. J.; Qin, C.; Trauger, S. A.; Brandon, T. R.; Custodio, D. E.; Abagyan, R.; Siuzdak, G. METLIN: a metabolite mass spectral database. *Ther. Drug Monit.* **2005**, *27*, 747.

(10) Want, E. J.; Maille, G. O.; Smith, C. A.; Brandon, T. R.; Uritboonthai, W.; Qin, C.; Trauger, S. A.; Siuzdak, G. Solvent-

dependent metabolite distribution, clustering, and protein extraction for serum profiling with mass spectrometry. *Anal. Chem.* **2006**, *78*, 743.
(11) Zenobi, R.; Knochenmuss, R. Ion formation in MALDI mass spectrometry. *Mass Spectrom. Rev.* **1998**, *17*, 337.
(12) Rainer, M.; Qureshi, M. N.; Bonn, G. K. Matrix-free and material-enhanced laser desorption/ionization mass spectrometry for the analysis of low molecular weight compounds. *Anal. Bioanal. Chem.* **2011**, *400*, 2281.
(13) Wei, J.; Buriak, J. M.; Siuzdak, G. Desorption−ionization mass spectrometry on porous silicon. *Nature* **1999**, *399*, 243.
(14) Kruse, R. A.; Li, X.; Bohn, P. W.; Sweedler, J. V. Experimental factors controlling analyte ion generation in laser desorption/ionization mass spectrometry on porous silicon. *Anal. Chem.* **2001**, *73*, 3639.
(15) Shen, Z.; Thomas, J. J.; Averbuj, C.; Broo, K. M.; Engelhard, M.; Crowell, J. E.; Finn, M. G.; Siuzdak, G. Porous silicon as a versatile platform for laser desorption/ionization mass spectrometry. *Anal. Chem.* **2001**, *73*, 612.
(16) Xiao, Y.; Retterer, S. T.; Thomas, D. K.; Tao, J.-Y.; He, L. Impacts of surface morphology on ion desorption and ionization in desorption ionization on porous silicon (DIOS) mass spectrometry. *J. Phys. Chem. C* **2009**, *113*, 3076.
(17) Ren, S.; Zhang, L.; Cheng, Z.; Guo, Y. Immobilized carbon nanotubes as matrix for MALDI-TOF-MS analysis: applications to neutral small carbohydrates. *J. Am. Soc. Mass Spectrom.* **2005**, *16*, 333.
(18) Wang, C.; Li, J.; Yao, S.; Guo, Y.; Xia, X. High-sensitivity matrix-assisted laser desorption/ionization Fourier transform mass spectrometry analyses of small carbohydrates and amino acids using oxidized carbon nanotubes prepared by chemical vapor deposition as matrix. *Anal. Chim. Acta* **2007**, *604*, 158.
(19) Go, E. P.; Apon, J. V.; Luo, G.; Saghatelian, A.; Daniels, R. H.; Sahi, V.; Dubrow, R.; Cravatt, B. F.; Vertes, A.; Siuzdak, G. Desorption/ionization on silicon nanowires. *Anal. Chem.* **2005**, *77*, 1641.
(20) Castaner, L.; Markvart, T. *Practical Handbook of Photovoltaics Fundamentals and Applications*, 1st ed.; Elsevier Science: New York, 2003.
(21) Raguin, D. H.; Morris, G. M. Antireflection structured surfaces for the infrared spectral region. *Appl. Opt.* **1993**, *32*, 1154.
(22) Wilson, S. J.; Hutley, M. C. The optical properties of "moth eye" antireflection surfaces. *Opt. Acta* **1982**, *7*, 993.
(23) Clapham, P. B.; Hutley, M. C. Reduction of lens reflexion by the "Moth Eye" principle. *Nature* **1973**, *244*, 281.
(24) Draine, B. T.; Flatau, P. J. User Guide for the Discrete Dipole Approximation Code DDSCAT 7.0., 2009; http://arxiv.org/abs/0809.0337v5.